JOURNAL OF GEOPHYSICAL RESEARCH, VOL. 107, NO. D19, 4367, doi:10.1029/2001JD001269, 2002

Physical properties of maritime low clouds as retrieved by combined use of Tropical Rainfall Measuring Mission (TRMM) Microwave Imager and Visible/Infrared Scanner
2. Climatology of warm clouds and rain

Hirohiko Masunaga,[1,2] Takashi Y. Nakajima,[1] Teruyuki Nakajima,[3] Misako Kachi,[1] and Kentaroh Suzuki[3]

Received 4 September 2001; revised 28 February 2002; accepted 25 March 2002; published 2 October 2002.

[1] In this paper, we investigate characteristics of low clouds and warm-rain production in terms of droplet growth based on the effective droplet radii retrieved by a combined use of visible, infrared, and microwave satellite remote sensing. We propose to categorize low clouds into the following groups: (1) nondrizzling, nonraining clouds; (2) nonraining clouds with drizzling near the cloud top; (3) raining clouds; and (4) clouds with no clear interpretation in terms of the effective radii derived using two different schemes. This categorization is supported by examination of the correlation between static stability and the retrieved results in the three "precipitating regions" (the Middle Pacific, South Pacific Convergence Zone [SPCZ], and Intertropical Convergence Zone [ITCZ] cumulus regions) and in the four "nonprecipitating regions" (the Californian, Peruvian, Namibian, and eastern Asian stratus regions). The rain rate derived by Precipitation Radar (PR) provides global characteristics consistent with our results. Californian and Peruvian stratus clouds are found to frequently have the drizzle mode near the cloud top, whereas Namibian strati have fewer chances to drizzle. The drizzle mode almost completely disappears in the eastern Asian region in the winter. The cloud–aerosol interaction is a promising candidate for suppressing the drizzle mode formation in nonprecipitating clouds. *INDEX TERMS:* 0320 Atmospheric Composition and Structure: Cloud physics and chemistry; 1610 Global Change: Atmosphere (0315, 0325); 1640 Global Change: Remote sensing; 1655 Global Change: Water cycles (1836)

Citation: Masunaga, H., T. Y. Nakajima, T. Nakajima, M. Kachi, and K. Suzuki, Physical properties of maritime low clouds as retrieved by combined use of Tropical Rainfall Measuring Mission (TRMM) Microwave Imager and Visible/Infrared Scanner, 2. Climatology of warm clouds and rain, *J. Geophys. Res.*, *107*(D19), 4367, doi:10.1029/2001JD001269, 2002.

1. Introduction

[2] A major climatological importance of clouds is their impact on the Earth's radiation budget. However, quantitative evaluation of the clouds' radiative effects on the Earth's climate involves numerous unknown factors. Clouds thus provide the largest uncertainty in predicting the future climate change such as global warming. Some of the difficulties lie in the geometrical complexity of clouds such as spatial inhomogeneity, brokenness, and overlapping. Possibly more essentially, problems arise from the lack of our knowledge of the response and sensitivity of the cloud physical properties to possible climate changes.

[3] Low stratiform clouds are known to play important roles as effective coolers of the Earth by reflecting solar radiation back to space, we hereafter designate low stratiform clouds containing stratus, stratocumulus, and fog simply as "stratus," after the notation by *Zuidema and Hartmann* [1995]. One may categorize low clouds into a few different types, depending on the formation mechanism and on the related environmental factors. *Klein and Hartmann* [1993] investigated the seasonal cycle of stratus and found that the appearance of low clouds is closely related with lower-tropospheric static stability. They identified ten regions of active stratocumulus convection, five of which are located off the west coasts of continents in the marine subtropics. In these areas, stratus clouds form over relatively cold sea surfaces where the trade inversion caps the boundary layer. One of the areas chosen by *Klein and Hartmann* [1993] is off the coast of California, where many marine stratus studies have been conducted both by in situ observations and by satellite remote sensing.

[4] Stratus clouds frequently also appear over the warm western boundary current in winter. Cold continental air blowing over the warm sea surface produces convective clouds triggered by the surface fluxes of heat and mois-

[1]Earth Observation Research Center, National Space Development Agency, Tokyo, Japan.
[2]Now at Department of Atmospheric Science, Colorado State University, Fort Collins, Colorado, USA.
[3]Center for Climate System Research, University of Tokyo, Tokyo, Japan.

0148-0227/02/2001JD001269$09.00

ture, where the inversion prevents the clouds from developing beyond the boundary layer. Stratocumuli in winter over the Sea of Japan, the East China Sea, and off the east coast of North America provide typical examples for this category.

[5] In contrast to nonprecipitating low clouds such as stratus, some maritime convective clouds at temperatures above freezing are capable of producing warm rain. Tropical clouds are known to constitute a broad spectrum of the cloud types. They consist of nonprecipitating shallow cumuli or trade wind cumuli, which dominate the cloud population, and by cumulonimbi, which dominate the convective rainfall [*Johnson et al.*, 1999, and references therein]. *Johnson et al.* [1999] suggested that cumulus congestus should be considered as the third component of the convective cloud spectrum in the tropics, based on statistics of radar-echo heights from the Tropical Ocean Global Atmosphere Coupled Ocean-Atmosphere Response Experiment (TOGA COARE) as well as other preceding studies. They pointed out that cumulus congestus, with detrainment through the cloud top near the 0°C stable layer, often forms precipitation by the warm-rain process.

[6] Maritime clouds are widely known to have relatively larger droplets with wider size spectra than continental clouds [*Squires*, 1958]. This is supported by more recent studies on the satellite-derived effective radius of liquid water clouds [*Han et al.*, 1994; *Kawamoto et al.*, 2001]. This tendency implies that maritime low clouds have higher potential to produce rainfall than continental clouds since the presence of large droplets enables collisional droplet growth, which is a necessary process following the diffusional-growth phase to form raindrops through the warm-rain process [*Rogers and Yau*, 1989]. Indeed, using satellite data, *Rosenfeld and Lensky* [1998] demonstrated that the collisional droplet growth takes place even near the cloud base for maritime clouds, while growth beyond the diffusional growth is rarely identified before glaciation starts for continental clouds. The cloud–aerosol interaction (see section 4.2) is believed to partly account for the difference in the cloud microphysical properties between maritime and continental clouds. A recent theory, however, showed that static stability (or updraft velocity at the cloud base) as well as the aerosol concentration is crucial to promote or suppress collisional growth [*Pinsky and Khain*, 2002].

[7] Impacts of clouds on the climate system involve various processes including radiative transfer, interactions with aerosols, and global hydrological cycles. To reveal cloud–climate interactions, we must therefore comprehensively understand the dynamic and microphysical processes of clouds as well as the radiative effects and complicated feedbacks among them. Our strategy is to clarify the climatological characteristics of low clouds and their dependence on environmental factors, in terms of the evolutionary status of droplet growth implied by satellite-derived effective radii. The purpose of the present paper is to make an overall examination of possible factors determining the physical state of low clouds. We leave future studies to go into more detail for responding to specific interests.

[8] *Masunaga et al.* [2002, hereafter referred to as Paper I] proposed a combined use of visible/infrared and microwave radiometers to derive the effective droplet radii by two different schemes. They found the results imply that the difference in those effective radii reflects a microphysical mechanism that expedites or suppresses the conversion of cloud water into rainfall. This paper is dedicated to a closer examination of the effective radii to identify the presence or absence of drizzle droplets and/or raindrops in low clouds.

[9] Section 2 outlines the retrieval algorithm and data adopted in this work. The results are presented in section 3. We discuss relations of our retrievals with the geographical features of rain rate and aerosols in section 4, and give the summary and conclusions in section 5.

2. Algorithm and Data

[10] This section briefly describes the retrieval scheme and data used in the present analysis. The major interest of this paper is to study the effective droplet radii (defined by equation (1) below) retrieved from satellite remote sensing over a wide spectral range from the visible to microwave. Similar strategies were employed by *Greenwald et al.* [1995] and *Zuidema and Hartmann* [1995], who used Special Sensor Microwave/Imager (SSM/I), International Satellite Cloud Climatology Project (ISCCP), and Earth Radiation Budget Experiment (ERBE) data to obtain liquid water path, cloudiness, and effective radius, respectively. *Lin et al.* [1998a, 1998b] studied the statistics of multilayered clouds and the effective radii in the use of SSM/I and Meteosat data.

[11] In Paper I, we proposed a new retrieval algorithm to simultaneously derive the effective radius, optical thickness, cloud top temperature, and liquid water path by a combined use of Visible and Infrared Scanner (VIRS) and TRMM Microwave Imager (TMI) aboard the Tropical Rainfall Measuring Mission (TRMM) satellite. This algorithm is outlined as follows. First, level 1 data of VIRS and TMI are assigned to the common global grid of 0.25 square degrees over oceans. Combining visible, near-infrared, and thermal infrared radiances (ch1, ch3, and ch4 of VIRS, respectively) yields the optical thickness, effective radius, and cloud top temperature [cf. *Nakajima and Nakajima*, 1995; *Kawamoto et al.*, 2001]. TMI brightness temperatures at 10.65GHz, 19.35GHz, and 37.0GHz are employed for evaluating the columnar water vapor (CWV) and liquid water path (LWP) on the grid points identified as cloudy by the VIRS analysis. The cloud top temperature obtained by the VIRS analysis is used in the TMI analysis to improve the accuracy in estimating LWP. Moreover, a cloud fraction correction is applied to reduce errors in LWP caused by difference in the spatial resolution between VIRS and TMI. The microwave-retrieved LWP with the optical thickness provides a different estimate of the effective radius from the VIRS analysis (section 3.1).

[12] As a minor technical change in the retrieval algorithm, we modified the way of incorporating the vertical profile of atmospheric water vapor in forward simulations for making a lookup table. Water vapor was assumed to decrease exponentially with increasing altitude under a constant scale height of 2.3 km in Paper I. In the present work, the water vapor is assumed to be mixed well, i.e., vertically homogeneous, below the cloud base and to

decrease linearly with increasing height toward the cloud top, above which water vapor content decays exponentially. The updated version is considered to represent the water vapor profile in cloudy atmospheres better than a fixed exponential profile as assumed before, although resultant retrievals were found to show no substantial changes due to the modification.

[13] Cold clouds with top temperatures below 273 K are omitted since the present analysis is focused on warm clouds. This criterion may be too strict to define warm clouds because very few ice crystals are detected in supercooled clouds considerably colder than 273 K. Dependence on the threshold temperature is discussed in section 4.3.

[14] As ancillary data required for the analysis, we adopt daily mean data of TMI-retrieved sea surface temperature (TMISST), provided by the Earth Observation Research Center of the National Space Development Agency of Japan (EORC NASDA). We also employ the global analysis (GANAL) data, which are six-hourly objective analysis archives provided by the Japan Meteorological Agency. A more detailed description of the retrieval scheme is given in Paper I. All the results in the present paper are based on two sets of three-monthly data, i.e., January, February, and March (JFM) 2000 and July, August, and September (JAS) 2000. We use the whole global data in section 3.2, as well as local-area data for the seven sites listed in Table 1 for the regional analysis in section 3.4. Note that we define "global" as the entire scene observable from the TRMM satellite, which covers ±38° in latitude.

[15] In addition to the satellite-derived cloud properties described above, global characteristics used to describe static stability are illustrated in section 3.2 below, where the temperature and humidity profiles are taken from National Center of Environmental Prediction (NCEP) Reanalysis data. The global distributions of rain rate near the surface and of the storm height shown in section 4.1 are taken from TRMM 3A25 products based on Precipitation Radar (PR) data.

3. Results

[16] The cloud physical properties retrieved by combined analysis of VIRS and TMI data are shown in this section. We first briefly summarize the results in Paper I (section 3.1). We then illustrate global features of low cloud properties retrieved by the present analysis and static stability calculated from NCEP Reanalysis data (section 3.2). We introduce our working hypothesis in section 3.3 to identify drizzle and rain in warm clouds, then examine regional features for seven representative sites (section 3.4).

3.1. A Brief Summary of Paper I

[17] Paper I introduced two different ways to derive the effective radius of cloud droplets,

$$R_e \equiv \frac{\int_0^\infty r^3 n(r) dr}{\int_0^\infty r^2 n(r) dr}, \quad (1)$$

where $n(r)$ is the droplet size distribution. The first-type effective radius is retrieved by using a pair of shortwave channels in visible and near-infrared bands [*Nakajima and King*, 1990; *Han et al.*, 1994; *Nakajima and Nakajima*, 1995; *Kawamoto et al.*, 2001], which is hereafter denoted by $R_{e(NV)}$. The second type effective radius is derived from the relation

$$R_{e(MV)} \equiv \frac{3\mathrm{LWP}_{micr}}{2\tau_c}, \quad (2)$$

where LWP_{micr} denotes the microwave-retrieved LWP, and τ_c, the optical thickness at a wavelength of 0.5 μm retrieved from shortwave analysis.

Table 1. Area Definitions of the Seven Representative Sites for Regional Analysis

Sites	Coverage	
Middle Pacific	160°E–180°E	10°N–25°N
ITCZ	120°W–100°W	5°N–15°N
SPCZ	120°W–100°W	20°S–10°S
Californian	130°W–120°W	20°N–30°N
Peruvian	90°W–80°W	20°S–10°S
Namibian	0°E–10°E	20°S–10°S
Eastern Asian	120°E–140°E	25°N–35°N

[18] The beam-filling efficiency should be considered to remove the cloud-inhomogeneity effect when microwave estimation of LWP is linked with the shortwave retrieval. In our scheme, the beam-filling efficiency is evaluated using the cloud fraction, which is defined by the number ratio of cloudy pixels to the total pixels derived from VIRS data. We performed the cloud-fraction correction before estimating LWP_{micr} to derive $R_{e(MV)}$ through equation (2). Paper I pointed out that the difference in those two effective radii could reflect a microphysical mechanism that expedites or suppresses the conversion of cloud water into rainfall. This implication is based on the intrinsic bias between $R_{e(NV)}$ and $R_{e(MV)}$, which arises from the spectral variation in the optical properties of water. Specifically, $R_{e(NV)}$ tends to be biased toward a value near the cloud top due to strong absorption of near-infrared radiation by water, while $R_{e(MV)}$ is expected to be close to the average in the whole cloud layer because microwave and visible radiation do not suffer from saturation within any cloud thickness of interest in the present work. The difference between $R_{e(NV)}$ and $R_{e(MV)}$ should therefore reflect the vertical inhomogeneity of droplet size inside the cloud, which is closely related with the microphysical process of droplet growth. Droplet size generally increases with increasing height and reaches a maximum near the top in a nonprecipitating cloud layer. In contrast, a precipitating cloud contains raindrops below or near the cloud base, and thus is detectable only by microwave measurement. In other words, $R_{e(MV)}$ should be smaller than $R_{e(NV)}$ for nonprecipitating low clouds, but the relation would be reversed once cloud drops grow large enough to precipitate.

[19] A major purpose of this paper is to closely examine $R_{e(MV)}$ and $R_{e(NV)}$ and give an overview of their dependence on the environmental factors and the microphysical properties of low clouds. In the next section, we discuss relations in global characteristics between static stability and the present retrievals.

3.2. Low Clouds and Static Stability

[20] The low cloud amount is positively correlated with lower-tropospheric static stability [*Klein and Hartmann*, 1993]. In this section, we present global trends of the low

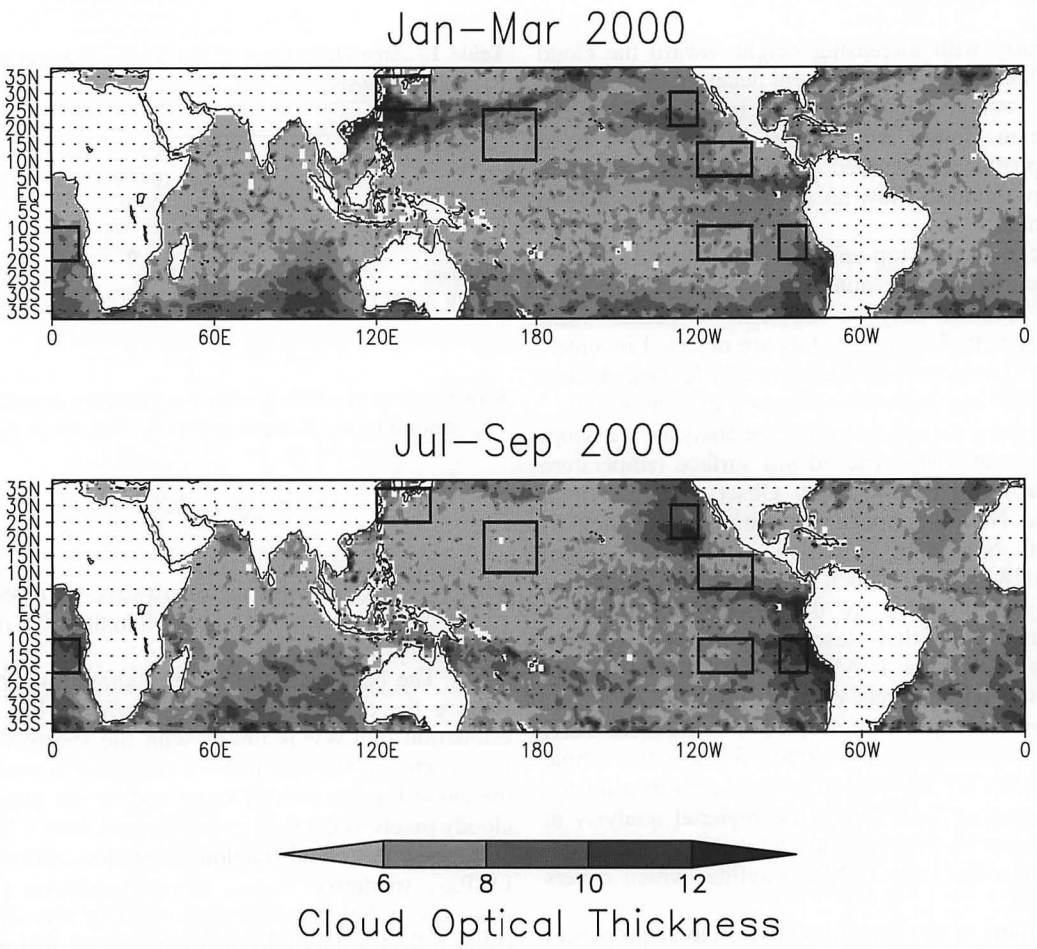

Figure 1. Cloud optical thickness (for clouds warmer than 273 K) retrieved by the VIRS analysis in three-monthly mean in JFM (upper) and in JAS (lower) 2000. Boxes shown in the figure indicate the sites listed in Table 1.

cloud distribution and demonstrate the relation with static stability based on a brief theory for cumulus convection described as follows.

[21] An adiabatic air parcel lifted by external force reaches the lifting condensation level (LCL) when water vapor inside the parcel is saturated and condensed into liquid water droplets. The base of a convective cloud therefore corresponds to LCL. In a conditionally unstable atmosphere, the cloud air parcel lifted further along the moist adiabat arrives at the level of free convection (LFC), beyond which the air parcel ascends by its own buoyancy without the help of an external force. The ascent of the air parcel is eventually halted when it looses its buoyancy at the level of neutral buoyancy (LNB), which roughly gives the cloud top height. LNB is expected to be low in altitude where the boundary layer is capped by the strong inversion. In contrast, LNB could be much higher near the tropopause in the tropical convergence zones. Furthermore, an LFC significantly lower in height than the freezing level may imply that cumulus convection would allow considerable droplet growth even for warm clouds, although warm rain is unlikely to form if LFC is so high close to LNB that strong updrafts of air promoting droplet growth are not expected.

[22] As an indicator of static stability or inversion strength, we calculated the atmospheric temperatures at LFC and LNB (hereafter denoted by the LFC temperature and the LNB temperature) from the NCEP Reanalysis data. The dry adiabatic lapse-rate is integrated to obtain the temperature within the air parcel, $T_p(z)$, from the surface to LCL, above which the integration is performed along the moist adiabat until it is equal to the ambient atmospheric temperature, $T_a(z)$. The altitude where $T_p(z)$ meets $T_a(z)$ first after the air parcel leaves the surface is defined as LFC. Further integration along the moist adiabat is performed until $T_p(z)$ reaches $T_a(z)$ again, where LNB is defined.

[23] Figure 1(2) shows the cloud optical thickness retrieved by our VIRS analysis (the LNB temperature) in three-monthly averages in JFM and JAS 2000. Note that the optical thickness in Figure 1 is that of low clouds because of the warm-cloud criterion, i.e., the cloud top temperature should exceed 273 K. Boxes in the figures represent the sites that we chose for regional analysis (summarized in Table 1), which is discussed in section 3.4. As mentioned in section 1, strong inversions, and thus low altitudes of LNB, are observed off the west coasts of continents in the subtropics, e.g., Californian, Peruvian, and Namibian areas. In these areas, the LNB temperature exceeds 0°C, and thus clouds are not allowed to develop beyond the freezing level. The optical thickness of low clouds (Figure 1) is relatively large, typically larger than 10, in those areas. This result is

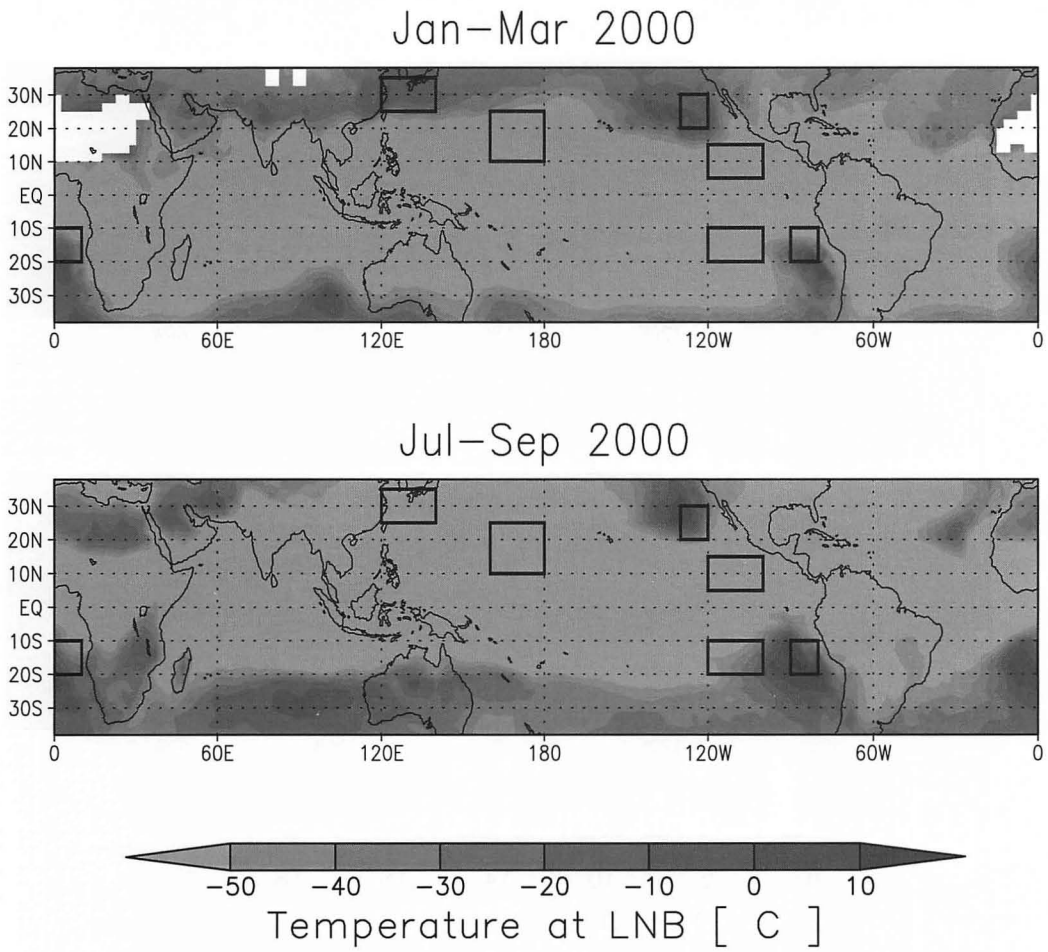

Figure 2. Temperature at the level of neutral buoyancy (LNB) calculated from NCEP Reanalysis data in three-monthly mean in JFM (upper) and in JAS (lower) 2000. Boxes shown in the figure indicate the sites listed in Table 1.

fully consistent with *Klein and Hartmann* [1993], who demonstrated that appearance of low clouds positively correlates with the inversion strength, although they used cloud amount and the potential temperature difference instead of optical thickness and the LNB temperature.

[24] The most prominent feature in Figure 1 is the horn-like structure with large optical thickness extending from the east coast of China to the midlatitude Pacific in JFM. As also mentioned in section 1, stratus clouds frequently appear in the East China Sea in winter, partly contributing to this structure. These low clouds, however, develop as blown eastward to deeper clouds capable of yielding heavy precipitation, and are eventually merged into the midlatitude storm track. The horn-like feature, especially near its tip, traces the southern edge of the storm track, where higher and thicker clouds typical of the storm track have been omitted from Figure 1 by the warm-cloud criterion.

[25] Figure 2 shows that the LNB temperatures over the tropical oceans are so low that convective clouds could be developed up to the tropopause. While deep convective clouds extending beyond the freezing level have been excluded from our analysis, shallower cumulus clouds warmer than 0°C, which are also major components of the tropical convective cloud spectrum (section 1), are within the scope of the present study. In contrast to stratus clouds that appear over the cold boundary currents, cumulus clouds over the tropical oceans are formed in a less stable atmosphere by virtue of a higher sea surface temperature and a higher humidity resulting in a higher LFC temperature. Figure 3 illustrates the LFC temperature calculated from the NCEP Reanalysis data. The LFC temperature is significantly higher than 0°C in the tropical oceans, which potentially allows rapid droplet growth in clouds even below the freezing level, which would enhance the probability of producing warm rain. On the other hand, the LFC temperature decreases almost to 0°C off the coasts of California, Peru, and Namibia. Recalling that these areas are subjected to a strong inversion, one can deduce that a free convection layer between LFC and LNB is so thin in these areas that droplet growth in a cloud layer would be less effective than in precipitating shallow clouds over the tropical oceans. A difference in the LFC temperature would therefore account for the regional variation in the capability of warm-rain production.

[26] Paper I inferred that precipitating clouds might be discriminated from nonprecipitating clouds by examining $R_{e(MV)}$ and $R_{e(NV)}$; clouds are expected not to be associated with significant precipitation if $R_{e(NV)}$ exceeds $R_{e(MV)}$, otherwise they are raining (section 3.1). Figure 4 draws the ratio of $R_{e(MV)}$ to $R_{e(NV)}$ retrieved from TRMM data.

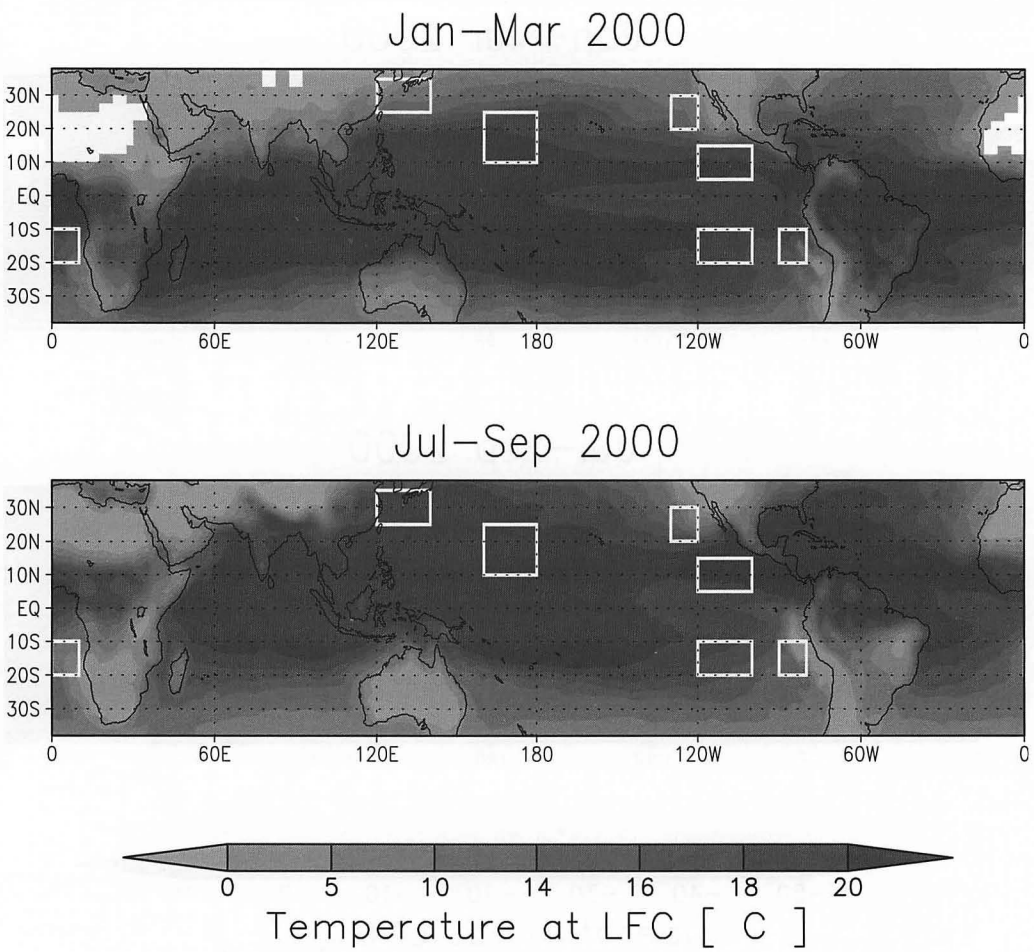

Figure 3. Same as Figure 2 but temperature at the level of free convection (LFC).

The global pattern in Figure 4 shows that precipitating regions such as the Intertropical and South Pacific Convergence Zones (ITCZ and SPCZ, respectively) are clearly traced by $R_{e(MV)}/R_{e(NV)}$ larger than unity. In contrast, $R_{e(MV)}/R_{e(NV)}$ is smaller than unity over the eastern boundary current, where the rain rate is much lower. The remarkable resemblance in patterns between Figures 3 and 4 supports the idea for correlation between $R_{e(MV)}/R_{e(NV)}$ and the presence of rainfall.

[27] Close examination of the Peruvian area in Figures 2 and 3 reveals that the domain having the maximum LNB temperature is detached from the coastline, with a narrow area between them showing the lowest LFC temperature. This narrow area shows the local maximum in cloud optical thickness (Figure 1) with the minimum in $R_{e(MV)}/R_{e(NV)}$ (Figure 4); these trends are more prominent in JAS. These facts suggest that clouds covering the area should contain very small droplets and be incapable of ascending from the sea surface, and thus they are probably fogs. Similar trends are also found in the Californian and Namibian areas, but they are not as evident as in the Peruvian area.

3.3. Detection of Drizzle and Rain

[28] In the previous section we showed that low clouds can be categorized to be precipitating or nonprecipitating in terms of the ratio of $R_{e(MV)}$ to $R_{e(NV)}$. We extend this idea in this section to include a category for drizzling clouds.

[29] The formation of warm rain begins with the onset of collisional droplet growth, which triggers generation of a separate peak at 100 μm in the droplet size spectrum, i.e., the drizzle mode [*Rogers and Yau*, 1989]. *Rosenfeld and Gutman* [1994] showed that 14 μm in $R_{e(NV)}$ is a threshold value above which clouds contain precipitation size hydrometeors using a satellite imager and weather radars. *Gerber* [1996] concluded that the threshold discriminating heavy-drizzle stratocumuli from light-drizzle ones is an effective radius of 16 μm using airborne probes. A detailed microphysical simulation for droplet growth illustrated that strong collisions start when effective radius attains about 15 μm [*Pinsky and Khain*, 2002]. These studies independently reached almost the same conclusion that the threshold for occurrence of drizzle is an effective radius of ~15 μm.

[30] Compiling all the implications given in the present and previous sections, we propose the following categorization in terms of $R_{e(NV)}$ and $R_{e(MV)}/R_{e(NV)}$, or the inverse of $\gamma \equiv R_{e(NV)}/R_{e(MV)}$ by the definition in Paper I, to identify nonprecipitating, drizzling, and precipitating clouds from satellite data. Figure 5 is a schematic illustration for the following categorization, where any given set of $R_{e(NV)}$ and $R_{e(MV)}/R_{e(NV)}$ specifies the category to which the cloud should belong.

1. The first category (domain 1 in Figure 5) is defined by $R_{e(NV)} < 15$ μm and $R_{e(MV)}/R_{e(NV)} < 1$. This type of cloud is not associated with drizzle mode or with precipitation.

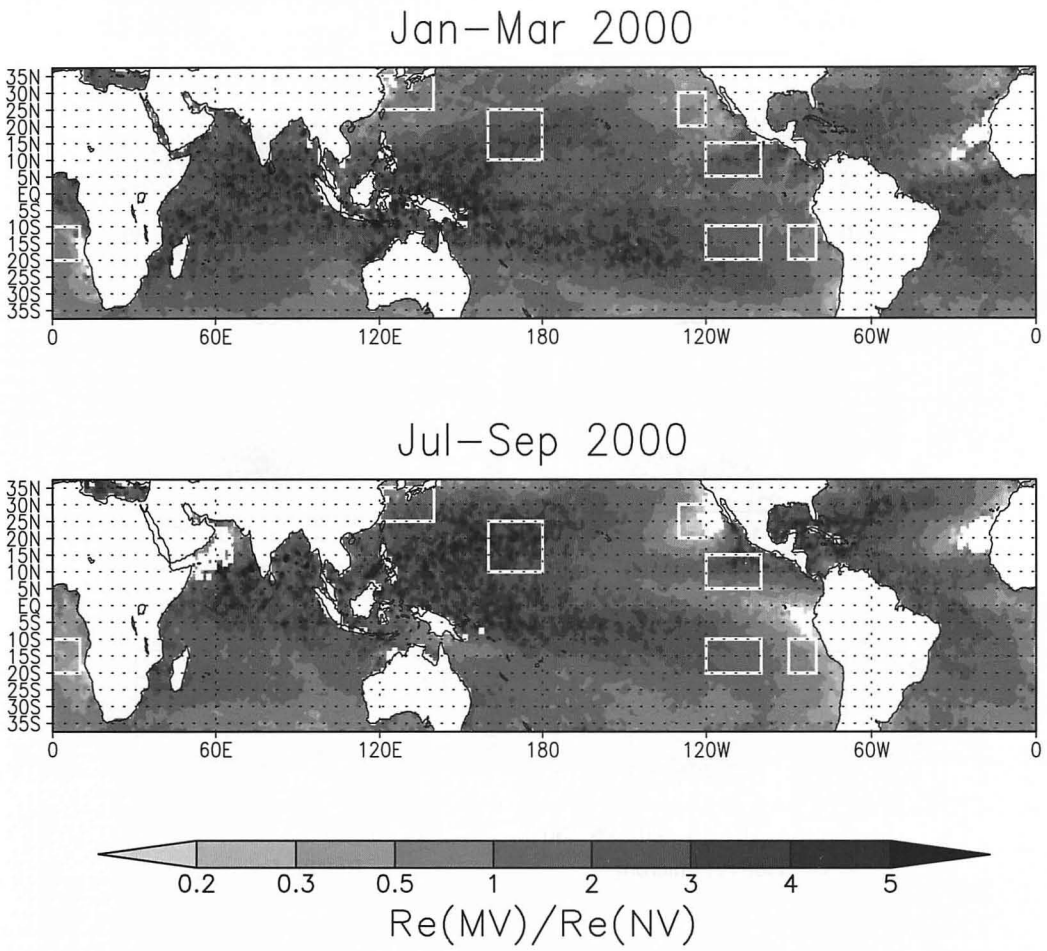

Figure 4. Ratio of $R_{e(MV)}$ to $R_{e(NV)}$ in three-monthly mean in JFM (upper) and in JAS (lower) 2000. Boxes shown in the figure indicate the sites listed in Table 1. See color version of this figure at back of this issue.

2. Clouds with $R_{e(NV)} > 15$ μm and $R_{e(MV)}/R_{e(NV)} < 1$ (domain 2) belong to the second category. The criterion of $R_{e(MV)} > 15$ μm implies that the clouds are probably drizzling, but the drizzle mode is confined to near the cloud top as long as $R_{e(MV)}/R_{e(NV)}$ remains below unity. Those clouds are unlikely to develop enough to produce considerable amounts of precipitation, although formation of the drizzle mode has begun near the cloud top through cumulus convection.

3. The third category consists of clouds with $R_{e(NV)} > 15$ μm and $R_{e(MV)}/R_{e(NV)} > 1$ (domain 3), which are expected to contain raindrops in appreciable numbers.

4. We do not have a convincing interpretation of the remaining category of $R_{e(NV)} < 15$ μm and $R_{e(MV)}/R_{e(NV)} > 1$ (domain 4). As a possible explanation, low precipitating clouds overlaid by nonprecipitating midlevel clouds may be fallen into this category [*Lensky and Rosenfeld*, 1997]. Validation studies, however, are necessary to confirm or reject this speculation.

[31] We apply our retrievals to this categorization in the subsequent section to figure out climatological characteristics on the microphysical states of low clouds.

3.4. Regional Characteristics

[32] Figures 6 (JFM) and 7 (JAS) show scatter diagrams for $R_{e(MV)}/R_{e(NV)}$ versus $R_{e(NV)}$ (cf. Figure 5). Each panel in Figure 6 gives statistics for each of the seven representative sites listed in Table 1 along with global statistics. We have omitted very tenuous clouds with optical thickness smaller than 4 in Figures 6 and 7 to reduce contamination of uncertainties in the surface emission seen through the cloud.

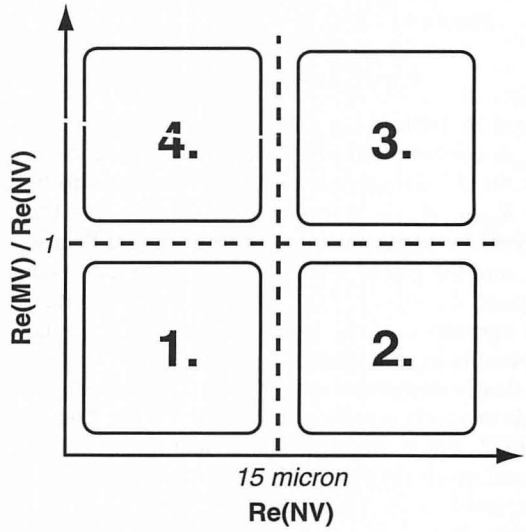

Figure 5. A schematic illustration to categorize the microphysical status of low clouds (see section 3.3 for details).

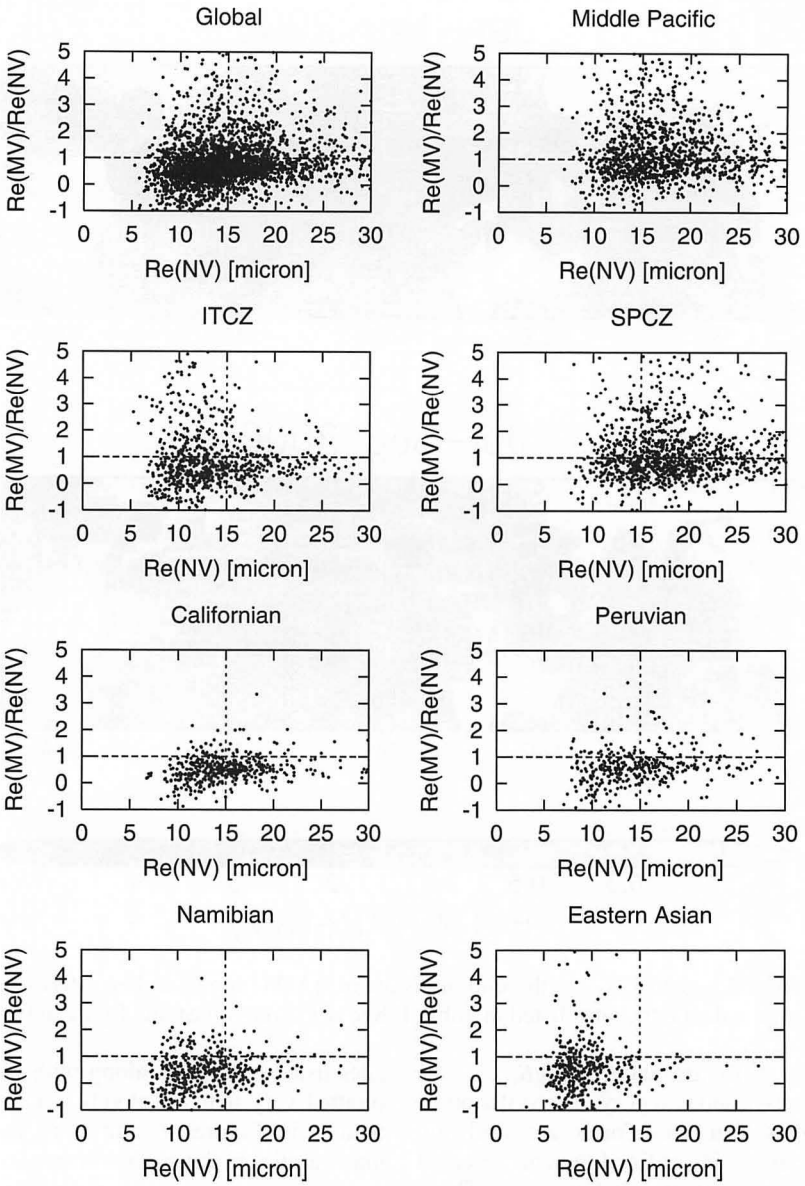

Figure 6. Ratio of $R_{e(MV)}$ to $R_{e(NV)}$ versus $R_{e\ (NV)}$ in JFM 2000. Location of each site is listed in Table 1.

Averages of $R_{e(MV)}$, $R_{e(NV)}$, and $R_{e(MV)}/R_{e(NV)}$ for each site are listed in Table 2.

[33] A common tendency identified throughout Figure 6 is that the density of scattered points appears to be largest where $R_{e(MV)}/R_{e(NV)}$ is equal to or slightly less than unity. However, the upper four panels (the Middle Pacific, ITCZ, SPCZ, and the global scene) contain many points dispersed far beyond the $R_{e(MV)}/R_{e(NV)} = 1$ line, whereas many fewer points surpass it in the lower four (the Californian, Peruvian, Namibian, and eastern Asian regions). This contrast is more clearly demonstrated in Table 2, where $R_{e(MV)}/R_{e(NV)}$ exceeds or nearly equals unity for the Middle Pacific, ITCZ, and SPCZ, but is slightly smaller than unity for the global mean and much smaller for the other four. This result, which is comparable to that in Figure 4, is fully consistent with the idea that $R_{e(MV)}/R_{e(NV)}$ reflects the probability of rain formation in low clouds.

[34] Figures 6 and 7 and Table 2 contain some negative values of $R_{e(MV)}$ and $R_{e(MV)}/R_{e(NV)}$ since microwave estimation of LWP could produce negative values because of uncertainties in the surface emissivity. Negative effective radii are physically meaningless, but we did not exclude them because LWP could be seriously overestimated if negative LWPs were excluded from statistics [*Lin and Rossow*, 1994].

[35] For convenience, we hereafter designate the Middle Pacific, ITCZ, and SPCZ as "precipitating regions" and the Californian, Peruvian, Namibian, and eastern Asian sites as "nonprecipitating regions." This classification is clearly defined depending on whether the average value of $R_{e(MV)}/R_{e(NV)}$ for each site is larger than the global mean or not (Table 2), and is supported as well by the global distribution of rain rate obtained from Precipitation Radar data (section 4.1). Figures 6 and 7 are examined below in more detail for each of the precipitating and nonprecipitating regions.

3.4.1. Precipitating Regions

[36] Table 2 shows that both $R_{e(MV)}$ and $R_{e(NV)}$ tend to have larger values in the precipitating regions than in the

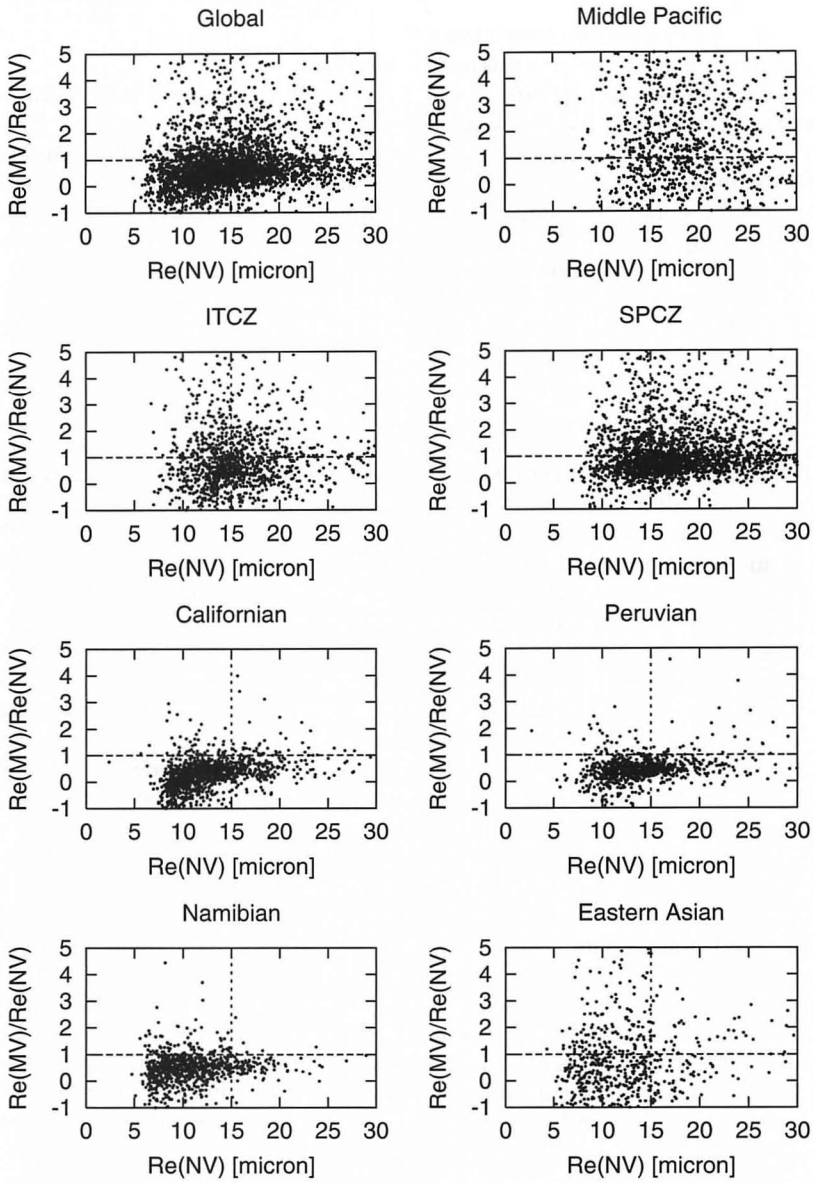

Figure 7. Same as Figure 6 but in JAS 2000.

nonprecipitating regions. The contrast between these two regions is more pronounced in $R_{e(MV)}$ than in $R_{e(NV)}$, which is responsible for the difference in variation of $R_{e(MV)}/R_{e(NV)}$. Large excess of $R_{e(MV)}$ over $R_{e(NV)}$ in the precipitating regions is considered to be attributed to the presence of raindrops (section 3.1).

[37] Among the precipitating regions, the smallest values are found in ITCZ for any of $R_{e(MV)}$, $R_{e(NV)}$, or their ratio both in JFM and in JAS in Table 2. This seemingly implies that ITCZ has the lowest probability of rain formation in low clouds among those three sites. However, it does not indicate that ITCZ provides less precipitation than SPCZ and the Middle Pacific because heavy precipitation over the tropical oceans is contributed mainly by deep convective clouds through the cold-rain process, which were excluded from our analysis by the warm-cloud criterion. Actually, the Middle Pacific and SPCZ by our definition are not the regions with heaviest precipitation in the tropics. (Note that the region defined as SPCZ in Table 1 is eastwardly off-centered from the usual notation.) Considerable seasonal variation is observed in the Middle Pacific, where data points are heavily dispersed (Figure 7) and $R_{e(MV)}$ is found even

Table 2. Three-Monthly Means of $R_{e(MV)}$ and $R_{e(NV)}$, and the Ratio of $R_{e(MV)}$ to $R_{e(NV)}$ for Each Site Listed in Table 1

Sites	JFM			JAS		
	$R_{e(MV)}$, μm	$R_{e(NV)}$, μm	Ratio	$R_{e(MV)}$, μm	$R_{e(NV)}$, μm	Ratio
Global	13.57	14.83	0.8637	12.40	14.90	0.7547
Middle Pacific	25.06	16.74	1.5181	30.85	17.86	1.7478
ITCZ	13.65	13.27	1.0766	13.63	15.38	0.8714
SPCZ	23.42	17.79	1.3227	21.24	17.31	1.2038
Californian	8.15	15.06	0.5155	3.32	12.55	0.1735
Peruvian	10.29	14.88	0.6577	6.78	14.04	0.4419
Namibian	3.86	12.83	0.2172	5.17	10.87	0.4354
East Asian	6.11	9.41	0.6292	1.34	12.11	−0.0491

larger (Table 2) for JAS, implying that precipitating clouds appear more frequently in summer than in winter in this area. Further interpretation of the $R_{e(MV)}/R_{e(NV)}$ versus $R_{e(NV)}$ diagram for the precipitating regions will be discussed in section 4.1.

3.4.2. Nonprecipitating Regions

[38] Table 2 illustrates that the nonprecipitating regions are separated from the precipitating regions by an average $R_{e(NV)}$ of 15 μm, which accords with the drizzle formation threshold (section 3.3). Closer examination of Figures 6 and 7 reveals that individual clouds frequently surpass 15 μm in $R_{e(NV)}$ in the Californian and Peruvian regions, indicating that low clouds often include the drizzle mode there. Drizzle droplets, however, are unlikely to grow into large raindrops because $R_{e(MV)}/R_{e(NV)}$ remains below unity in most cases even when the drizzle mode is identified near the cloud top. Compared to the Californian and Peruvian regions, the drizzle mode is less frequently identified in the Namibian region and it almost completely disappears in the eastern Asian region in JFM. The drizzle mode in those regions may be quenched by the cloud–aerosol interaction. We will revisit this subject in section 4.2. There could be other meteorological factors that suppress the drizzle mode, but we consider that the cloud–aerosol interaction is the most plausible candidate for the following reasons.

[39] First, the Californian, Peruvian, and Namibian stratus regions are under similar meteorological conditions, i.e., over cold boundary currents off the west coasts of the continents, while only eastern Asian stratus is formed over the warm current off the east coast. This difference in the meteorological conditions could not account for the contrast between Californian/Peruvian regions and the Namibian/eastern Asian regions. Second, if the suppression of the drizzle mode as seen in the eastern Asian and Namibian regions is not due to large CCN concentrations, a difference in static stability should be responsible for suppressing the droplet growth. Figures 2 and 3, however, show no notable evidence for a difference in static stability, or in LNB and LFC temperatures, between the Namibian/eastern Asian regions and the other two stratus regions.

[40] Extremely small values of $R_{e(MV)}$ seen in Namibian and eastern Asian regions (Table 2) are observed in broken clouds with low LWP and small cloud fractions, e.g., fair-weather cumulus. In such cases, microwave estimation of LWP is liable to suffer from relatively large errors because of uncertainties in the surface emissivity. Therefore, reliability of $R_{e(MV)}$ may not be ensured when it shows an exceptionally small value, but this does not seriously damage our conclusive remarks.

4. Discussions

4.1. Rain Rate Near Surface Rain Rate

[41] The previous section was devoted to illustrating that an idea proposed in section 3.3 is supported by the retrievals from satellite observations shown in Figures 6 and 7, which is consistent with the geographical characteristics in lower-tropospheric static stability. In this section, we investigate the correlation between raining and/or drizzling clouds identified by our classification and rainfall observed by Precipitation Radar (PR) aboard the TRMM satellite.

[42] PR data should have been omitted when the cloud top temperature is lower than 273 K for comparing our results directly with the PR rain rate. However, we present the total rainfall without screening in Figure 8 because the purpose of this section is not only validating our results but also showing the climatological characteristics of warm rain in the context of the total rainfall. The rain type (cold or warm) is indicated in terms of the storm height, which is defined by the altitude of the highest radar echo detected by PR.

[43] Figure 8 shows the three-monthly mean rain rate near the surface derived from PR along with the atmospheric temperature at the storm height (hereafter called storm-height temperature). We calculated the storm-height temperature assuming a temperature lapse-rate of 6.5 K/km from sea surface temperature (and hence the storm-height temperature is drawn only over oceans in Figure 8). Storm-height temperatures substantially above 0°C indicate that warm rain dominates the precipitation processes in that region, whereas cold rain is likely if the storm-height temperature is far below 0°C. Although this latter statement is not always true because liquid water hydrometeors often exist below temperatures of −15°C, the storm-height temperature provides a tentative guideline to roughly illustrate regional trends of precipitation processes. Note that PR is not sensitive to ice particles unless they have grown very large, and therefore the storm height for cold rain only gives the lower limit for the actual height at which precipitation begins.

[44] Among the nonprecipitating regions identified in section 3.4 above, the Californian, Peruvian, and Namibian areas are confirmed to have rain rates of less than 1 mm/hr, which is comparable to the lower detection limit of rainfall by PR. California in JFM appears to have slightly higher rain rates than in JAS since the midlatitude storm track is shifted southward (closer to this site) in JFM as seen in Figure 8. Peru does also under the influence of doubled ITCZ in JFM. This seasonal variation is consistent with Table 2, where the ratio of effective radii is larger in JFM than in JAS for both of the Californian and Peruvian sites. The eastern Asian area is found to have considerable rainfall with rain rates of 2–5 mm/hr, even though it is categorized as a nonprecipitating region. This seems to be a contradiction, but it actually is not, because rainfall in the midlatitude is mainly due to the cold-rain process and most warm clouds found there are nonprecipitating. Figure 8 shows that the storm-height temperature in eastern Asia is indeed lower than 0°C.

[45] The precipitating regions can be divided into two categories by average rain rates, heavily precipitating areas with typical rain rates exceeding 2 mm/hr (Middle Pacific in JAS and ITCZ) and moderately precipitating areas (Middle Pacific in JFM and SPCZ). We again notice that the region "SPCZ" by our definition (Table 1) is off-center from the area with heaviest precipitation in the South Pacific. The moderately precipitating regions have storm-height temperatures above 10°C, strongly indicating that rainfall in those regions is dominated by the warm-rain process from precipitating shallow clouds. In contrast, correlation between the classification proposed in Figure 5 and rain rate is less

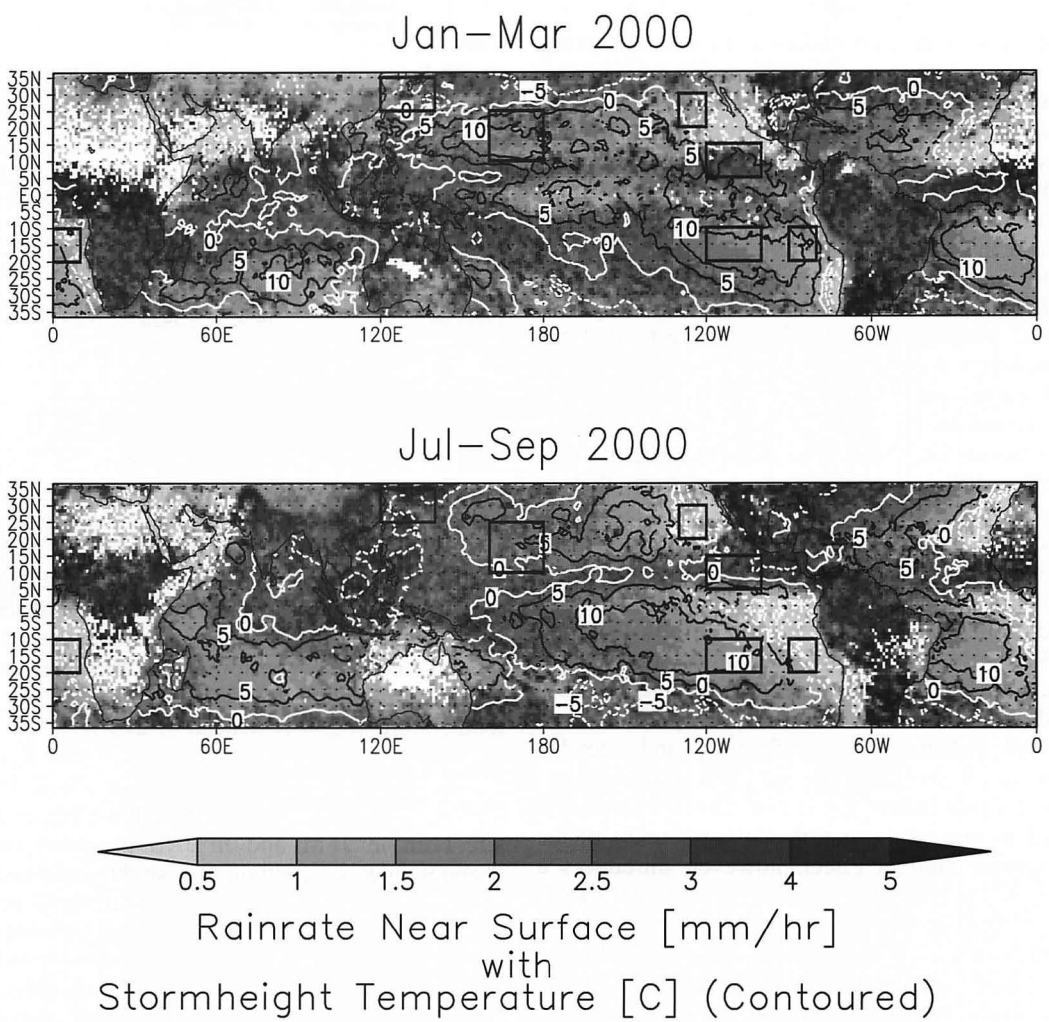

Figure 8. Three-monthly-mean rain rate near the surface derived from PR in JFM (upper) and JAS (lower) 2000. Contours delineate the atmospheric temperature at the storm height, which is calculated from the PR storm height on the assumption of a temperature lapse-rate of 6.5 K/km from sea surface temperature given by TMISST. Red-colored and purple-colored contours denote the storm-height temperatures beyond and below 0°C, respectively. Boxes shown in the figure indicate the sites listed in Table 1. See color version of this figure at back of this issue.

clear in heavily precipitating regions since deep convective clouds play significant roles in the total rainfall through the cold-rain process. In fact, it is curious that ITCZ shows only a weak sign of rainfall in Table 2, compared to less precipitating regions such as SPCZ and the Middle Pacific. A possible explanation for this tendency is that subsidence from coexisting deep convection may tend to suppress growth of neighboring shallow clouds. However, further examination of the dynamical interaction among tropical cumulus clouds is outside the scope of the present study.

[46] We avoided choosing the rainiest region in the tropics, e.g., the western Pacific warm pool, as a representative site because low clouds over the warm pool were very infrequently detected. This is the same reason why we have shifted our "SPCZ" eastward from the usual definition. This is presumed to be attributed to frequent appearance of high clouds obscuring lower clouds in those areas where active deep convection moistens the upper troposphere. We have indeed confirmed that frequency of low-cloud detection increases with decreasing threshold temperature for the warm-cloud criterion over the warm pool (not shown). More detailed investigation involved with the cloud overlapping, however, is also beyond the scope of this work and is thus left for future studies.

4.2. Interaction With Aerosols

[47] We showed in section 3.4.2 that the drizzle mode is suppressed for stratus clouds in the Namibian and eastern Asian regions, in contrast to the Californian and Peruvian stratus regions. It was also implied there that the cloud–aerosol interaction is a candidate for suppressing the drizzle mode. The cloud–aerosol interaction is increasing in climatological importance because it plays important roles both in the cloud microphysics and in influencing the Earth's radiation budget, i.e., the aerosol indirect effect, as described below. This section is devoted to introducing the cloud–aerosol interaction and to discus-

sing the relation between past studies and the results of this paper.

[48] Hydrophilic aerosols activated as cloud condensation nuclei (CCN) affect the cloud physical properties. *Twomey* [1977] showed that an increase of the aerosol concentration enhances the cloud reflectivity in the global average. *Coakley et al.* [1987] and *Radke et al.* [1989] confirmed enhancement of the cloud reflectivity due to the ship track effluence, and *Kaufman and Fraser* [1997] found the same trend caused by carbonaceous aerosols generated by biomass burning. *Nakajima et al.* [2001] investigated the correlation between the cloud and aerosol concentrations by means of global analysis of satellite data. *Bréon et al.* [2002] also found that the effect of aerosols on cloud microphysics occurs on a global scale using satellite data by means of a different retrieval scheme from that of *Nakajima et al.* [2001].

[49] In addition to changes in the cloud reflectivity, the shrinking of cloud droplets in response to an increase in the aerosol concentration would suppress the formation of drizzle, and hence would extend the cloud lifetime [*Albrecht*, 1989]. By a combined use of the radiometers and radars aboard the TRMM satellite, *Rosenfeld* [2000] demonstrated that urban and industrial air pollution can suppress rainfall. Enhanced cloud reflectivity and extended cloud lifetime as a result of interaction with aerosols is known as the aerosol indirect effect, which has become to be recognized as one of the major cooling sources of the Earth. The aerosol indirect effect, however, introduces a large uncertainty in predicting global warming [*IPCC01*, 2001].

[50] It is interesting to compare the findings by *Nakajima et al.* [2001] with occurrence or disappearance of the drizzle mode in the nonprecipitating regions as discussed in section 3.4, although their analysis is based on annual-mean retrievals in 1990. According to *Nakajima et al.* [2001], the strongest positive correlation between the number concentrations of cloud droplets and aerosols was found over the East China Sea, which infers that numerous anthropogenic aerosols emitted from China cause cloud droplets to shrink in the surrounding areas. Evidence of the cloud–aerosol interaction was also identified off the west coast of Namibia, and less clearly over the ocean near Peru, but no sign of such interactions was found in the Californian area. Recalling the findings in section 3.4, where drizzling clouds are frequently found in the Californian and Peruvian regions but less frequently in the Namibian and completely disappear in the eastern Asian, one finds that the cloud–aerosol interaction is a promising candidate for dominating droplet growth in nonprecipitating clouds, for which a high aerosol concentration suppresses the drizzle mode.

4.3. Dependence on the Warm-Cloud Criterion

[51] Clouds with top temperatures below 273 K have been omitted from our analysis since the present study is focused on liquid water clouds. Clouds, however, often contain supercooled water droplets even if the water temperature is considerably lower than 0°C. Cloud droplets are known to freeze spontaneously at temperatures as low as −40°C, whereas ice crystals usually appear in a cloud in appreciable numbers when the temperature drops below −15°C through heterogeneous nucleation [*Rogers and Yau*, 1989]. There is a wide variety in actual clouds at temperatures between 0°C and −40°C, depending on whether cloud particles are in the purely liquid phase, purely ice phase, or a mixed phase. Our threshold of 273 K assures a sufficient condition for clouds to be in the liquid phase and may be overly strict in some cases. To estimate dependence of the threshold temperature on the statistics of the retrieved effective radius, we performed another analysis in the same way as presented in section 3.4 except for a threshold temperature at 258 K instead of 273 K.

Table 3. Same as Table 2 Except for the Threshold Temperature of 258 K for the Warm-Cloud Criterion Instead of 273 K

Sites	JFM			JAS		
	$R_{e(MV)}$, μm	$R_{e(NV)}$, μm	Ratio	$R_{e(MV)}$, μm	$R_{e(NV)}$, μm	Ratio
Global	10.50	15.07	0.6602	9.16	15.34	0.5347
Middle Pacific	19.73	16.50	1.1904	11.28	17.73	0.6108
ITCZ	8.61	14.06	0.6589	7.90	15.80	0.4636
SPCZ	19.89	17.88	1.1223	20.03	17.31	1.1308
Californian	7.32	15.08	0.4587	2.36	12.57	0.0930
Peruvian	8.78	14.92	0.5456	6.30	14.05	0.4046
Namibian	1.77	12.87	0.0418	4.60	10.84	0.3781
Eastern Asian	5.65	10.16	0.5518	−5.25	13.84	−0.4875

[52] Table 3 lists averages of $R_{e(MV)}$ and $R_{e(NV)}$, and their ratio for the threshold temperature of 258 K. In comparison with Table 2, the decreased threshold temperature at every site both in JFM and in JAS produces no significant changes in $R_{e(NV)}$, although a slightly increasing tendency of about 1 μm with decreasing threshold temperature is observed in the eastern Asian region. In contrast, $R_{e(MV)}$ is considerably decreased by the decreased threshold temperature. This correlation of $R_{e(MV)}$ with the threshold temperature is accounted for by the increasing contribution of ice crystals as the cloud temperature decreases. For clouds containing an ice-water mixture, the estimate of $R_{e(MV)}$ using equation (2) should be rewritten as

$$R_{e(MV)} \equiv \frac{3\mathrm{TWP}}{2\tau_c}, \tag{3}$$

where TWP stands for the total water path including both liquid and ice water. However, microwave sensors would miss the ice water component because of their insensitivity to ice crystals, which results in underestimation of $R_{e(MV)}$ in equation (3). As a consequence, we prefer the threshold temperature of 273 K as the warm-cloud criterion in order to avoid underestimating $R_{e(MV)}$ due to contamination of ice crystals.

5. Summary and Conclusions

[53] In this paper, we investigate the characteristics of low clouds and warm-rain production in terms of droplet growth in warm clouds, based on the effective droplet radii retrieved by a combined use of visible, infrared, and microwave satellite remote sensing. The present study is focused on an overall examination, and thus more detailed investigations of specific factors such as the cloud–aerosol interaction are left to future work.

[54] The retrieval algorithm, described in detail in Paper I, is designed to be applied to VIRS and TMI aboard the

TRMM satellite to evaluate the cloud optical thickness, cloud top temperature, LWP, and the cloud effective radii. In particular, LWP and the effective radius are derived in the two different ways using visible and infrared radiances and the combination of visible radiance and microwave brightness temperatures. These two effective radii, $R_{e(NV)}$ and $R_{e(MV)}$, do not accord with each other in general because $R_{e(NV)}$ tends to be biased toward the value near cloud top while $R_{e(MV)}$ is close to the average within the whole cloud layer. The ratio of those two effective radii, $R_{e(MV)}/R_{e(NV)}$, is therefore expected to represent the vertical inhomogeneity of the effective radius in a cloud layer. For nonprecipitating cumulus, the mean droplet size is known to increase with increasing height due to droplet growth and coalescence in an ascending air parcel, and hence $R_{e(MV)}$ would be slightly smaller than $R_{e(NV)}$. In contrast, $R_{e(MV)}/R_{e(NV)}$ should exceed unity if clouds produce raindrops that fall below the cloud base. These considerations, along with observational and theoretical implications by past studies, lead us to categorize low clouds into the following four groups: (1) nondrizzling, nonraining clouds ($R_{e(NV)} < 15$ μm, $R_{e(MV)}/R_{e(NV)} < 1$), (2) nonraining clouds with drizzling near the cloud top ($R_{e(NV)} > 15$ μm, $R_{e(MV)}/R_{e(NV)} < 1$), (3) raining clouds ($R_{e(NV)} > 15$ μm, $R_{e(MV)}/R_{e(NV)} > 1$) (section 3.3), and (4) other clouds ($R_{e(NV)} < 15$ μm and $R_{e(MV)}/R_{e(NV)} > 1$) with no clear interpretation. Low raining clouds with overlying nonprecipitating clouds might belong to this final category, but we have no verification.

[55] We chose seven representative sites for the regional analysis (Table 1). The Californian, Peruvian, and Namibian sites are characterized by optically thick stratus clouds (Figure 1), which are capped by a strong inversion as indicated by calculated LNB (level of neutral buoyancy, Figure 2). This is consistent with the findings by *Klein and Hartmann* [1993]. All of those sites exhibit values of $R_{e(MV)}/R_{e(NV)}$ less than unity in average (Figure 4 and Table 2), which supports our categorization. Californian and Peruvian stratus clouds are found to often surpass 15 μm in $R_{e\,(NV)}$ or, in other words, to frequently have the drizzle mode near the cloud top, whereas Namibian strati have fewer chances to drizzle. Stratus clouds are abundant also in the eastern Asian region in winter, but occurrence of the drizzle mode is rarely identified there in contrast to the other three stratus regions. The cloud–aerosol interaction is a promising candidate for suppressing formation of the drizzle mode in nonprecipitating clouds (section 4.2).

[56] The Californian, Peruvian, Namibian and eastern Asian stratus regions, designated as "nonprecipitating regions" for convenience, are distinguished from "precipitating regions", comprised of the Middle Pacific, ITCZ, and SPCZ cumulus regions, depending on whether the average value of $R_{e(MV)}/R_{e(NV)}$ is smaller or larger than the global mean (Table 2).

[57] Warm-rain production requires an unstable layer below the freezing level so thick as to allow the collisional droplet growth to yield raindrops. The rain rate near the surface obtained by PR shows that the Middle Pacific in JFM and SPCZ (at its eastern edge by our definition) have moderate rainfall. In these regions, deep convective clouds that form heavy precipitation through the cold-rain process do not appear frequently because of the trade inversion, and warm rain is the only source to provide precipitation. Precipitating shallow cumuli such as congestus clouds that do not develop far beyond the 0°C layer probably contribute to warm rain in the tropics [*Johnson et al.*, 1999]. Further studies are necessary for tropical regions with heavier precipitation, e.g., the western Pacific warm pool (not shown in this work) and ITCZ, since the present work is focused on low clouds and the warm-rain process.

[58] The above findings all lead us to the following general conclusions on the mechanism determining the microphysical state of low clouds.

1. Based on combined analysis of shortwave and microwave measurements, nondrizzling clouds, drizzling clouds, and raining clouds are discriminated on the two-dimensional plane constructed by $R_{e(NV)}$ and $R_{e(MV)}/R_{e(NV)}$.
2. Nonprecipitating clouds are composed of drizzling (but not raining) clouds and nondrizzling clouds. Although both types of nonprecipitating clouds are formed under the strong inversion over the boundary current, the drizzle mode is suppressed if any external forcing is exerted to prevent droplet growth, probably by the presence of abundant aerosols.
3. The drizzle mode can be converted into warm rain over the tropical and subtropical oceans having high sea surface temperature and high humidity.

[59] There remain many unresolved issues. Detailed investigation of the cloud–aerosol interaction for nonprecipitating stratus clouds was beyond the scope of the present study. Moreover, the conversion efficiency from the drizzle mode to warm rain would be affected by the aerosol concentration as well as the surface temperature and humidity for continental and coastal clouds [*Rosenfeld*, 2000]. To investigate the radiative effects of clouds on climate, cloud lifetime as well as droplet size should be estimated from the efficiency of conversion from clouds into rainfall. Middle and high clouds, as well as low clouds, should be included inside the scope to discuss the Earth's energy budget in total, which involves studying the cold-rain process in addition to the warm-rain process. These are formidable issues to resolve, but some of them will be subjects in our subsequent work.

[60] **Acknowledgments.** VIRS(1B01), TMI(1B11) and PR(3A25) data were provided by NASA Goddard Space Flight Center, and GANAL data by the Japan Meteorological Agency. TMISST (Version 2.0) was produced and supplied by NASDA Earth Observation Research Center. NCEP Reanalysis data were provided by the NOAA-CIRES Climate Diagnostics Center, Boulder, Colorado, USA.

References

Albrecht, B. A., Aerosols, cloud microphysics, an fractional cloudiness, *Science*, *245*, 1227–1230, 1989.

Brenguier, J.-L., H. Pawlowska, L. Schüller, R. Preusker, J. Fischer, and Y. Fouquart, Radiative properties of boundary layer clouds: Droplet effective radius versus number concentration, *J. Atmos. Sci.*, *57*, 803–821, 2000.

Bréon, F. M., D. Tanré, and S. Generoso, Aerosols effect on cloud droplet size monitored from satellite, *Science*, *295*, 834–838, 2002.

Coakley, J. A., Jr., R. K. Bernstein, and P. A. Durkee, Effect of ship-track effluents on cloud reflectivity, *Science*, *237*, 1020–1022, 1987.

Gerber, H., Microphysics of marine stratocumulus clouds with two drizzle modes, *J. Atmos. Sci.*, *53*, 1649–1662, 1996.

Greenwald, T. J., G. L. Stephens, S. A. Christopher, and T. H. Vonder Haar, Observations of the global characteristics and regional radiative effects of marine cloud liquid water, *J. Clim.*, *8*, 2928–2946, 1995.

Han, Q., W. B. Rossow, and A. A. Lacis, Near-global survey of effective

droplet radii in liquid water cloud using ISCCP data, *J. Clim.*, *7*, 465–497, 1994.

IPCC01, in *Climate Change 2001—The Scientific Basis*, edited by J. T. Houghton, Cambridge Univ. Press, New York, 2001.

Johnson, R. H., T. M. Rickenbach, S. A. Rutledge, P. E. Ciesielski, and W. H. Schubert, Trimodal characteristics of tropical convection, *J. Clim.*, *12*, 2397–2418, 1999.

Kaufman, Y. J., and R. S. Fraser, The effect of smoke particles clouds and climate forcing, *Science*, *277*, 1636–1639, 1997.

Kawamoto, K., T. Nakajima, and T. Y. Nakajima, A global determination of cloud microphysics with AVHRR remote sensing, *J. Clim.*, *14*, 2054–2068, 2001.

Klein, S. A., and D. L. Hartmann, The seasonal cycle of low stratiform clouds, *J. Clim.*, *6*, 1587–1606, 1993.

Lensky, I. M., and D. Rosenfeld, Estimation of precipitation are and rain intensity based on the microphysical properties retrieved from NOAA AVHRR data, *J. Appl. Meteorol.*, *36*, 234–242, 1997.

Lin, B., and W. B. Rossow, Observations of cloud liquid water path over oceans: Optical and microwave remote sensing methods, *Geophys. J.*, *99*, 20,907–20,927, 1994.

Lin, B., B. Wielicki, P. Minnis, and W. Rossow, Estimation of water cloud properties from satellite microwave, infrared and visible measurements in oceanic environments, 1, Microwave brightness temperature simulations, *J. Geophys. Res.*, *103*, 3873–3886, 1998a.

Lin, B., P. Minnis, B. Wielicki, D. R. Doelling, R. Palikonda, D. F. Young, and T. Uttal, Estimation of water cloud properties from satellite microwave, infrared and visible measurements in oceanic environments, 2, Results, *J. Geophys. Res.*, *103*, 3887–3905, 1998b.

Masunaga, H., T. Y. Nakajima, T. Nakajima, M. Kachi, R. Oki, and S. Kuroda, Physical properties of maritime low clouds as retrieved by combined use of Tropical Rainfall Measurement Mission Microwave Imager and Visible/Infrared Scanner, 2, Algorithm, *J. Geophys. Res.*, *107*, 10.1029/2001JD000743, 2002.

Nakajima, T., and M. D. King, Determination of the optical thickness and effective particle radius of clouds reflected solar radiation measurements, 1, Theory, *J. Atmos. Sci.*, *47*, 1878–1893, 1990.

Nakajima, T., A. Higurashi, K. Kawamoto, and J. E. Penner, A possible correlation between satellite-derived cloud and aerosol microphysical parameters, *Geophys. Res. Lett.*, *28*, 1171–1174, 2001.

Nakajima, T. Y., and T. Nakajima, Wide-Area determination of cloud microphysical properties from NOAA AVHRR measurement for FIRE and ASTEX regions, *J. Atmos. Sci.*, *52*, 4043–4059, 1995.

Pinsky, M. B., and A. P. Khain, Effects of in-cloud nucleation and turbulence on droplet spectrum formation in cumulus clouds, *Q. J. R. Meteorol. Soc.*, *128*, 501–534, 2002.

Rogers, R. R., and M. K. Yau, *A Short Course in Cloud Physics*, 3rd ed., 290 pp., Butterworth-Heinemann, Woburn, Mass., 1989.

Rosenfeld, D., Suppression of rain and snow by urban and industrial air pollution, *Science*, *287*, 1793–1796, 2000.

Rosenfeld, D., and G. Gutman, Retrieving microphysical properties near the tops of potential rain clouds by multispectral analysis of AVHRR data, *J. Atmos. Sci.*, *34*, 259–283, 1994.

Rosenfeld, D., and I. M. Lensky, Satellite-based insights into precipitation formation processes in continental and maritime convective clouds, *Bull. Am. Meteorol. Soc.*, *79*, 2457–2476, 1998.

Squires, P., The microstructure and colloidal stability of warm clouds, 1. The relation between structure and stability, *Tellus*, *10*, 256–261, 1958.

Twomey, S., The influence of pollution on the shortwave albedo of clouds, *J. Atmos. Sci.*, *34*, 1149–1152, 1977.

Zuidema, P., and D. L. Hartmann, Satellite determination of stratus cloud microphysical properties, *J. Clim.*, *8*, 1638–1657, 1995.

M. Kachi and T. Y. Nakajima, Earth Observation Research Center. National Space Development Agency, Tokyo 104-6023, Japan.

H. Masunaga, Department of Atmospheric Science, Colorado State University, Fort Collins, CO 80523, USA. (masunaga@atmos.colostate.edu)

T. Nakajima and K. Suzuki, Center for Climate System Research. University of Tokyo, 4-6-1 Komaba, Meguro-ku, Tokyo 153-8904, Japan.

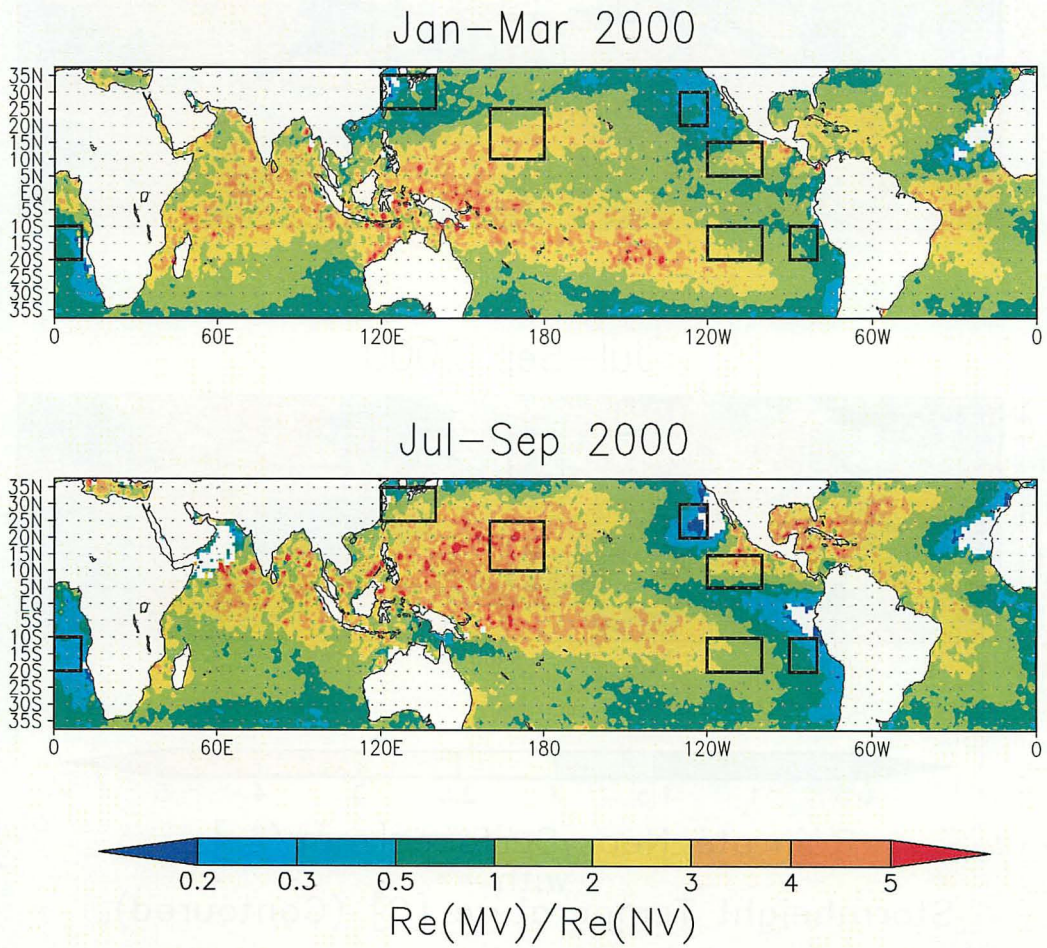

Figure 4. Ratio of $R_{e(MV)}$ to $R_{e(NV)}$ in three-monthly mean in JFM (upper) and in JAS (lower) 2000. Boxes shown in the figure indicate the sites listed in Table 1.

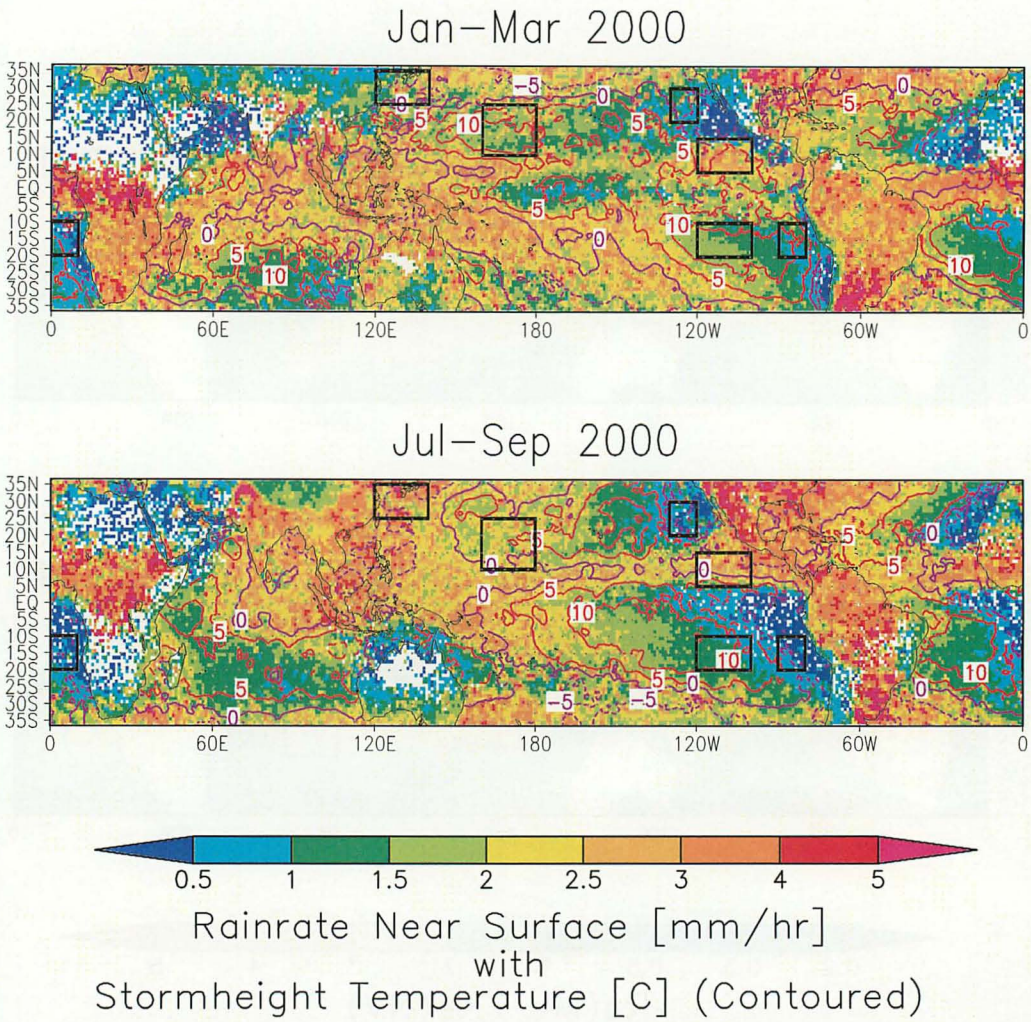

Figure 8. Three-monthly-mean rain rate near the surface derived from PR in JFM (upper) and JAS (lower) 2000. Contours delineate the atmospheric temperature at the storm height, which is calculated from the PR storm height on the assumption of a temperature lapse-rate of 6.5 K/km from sea surface temperature given by TMISST. Red-colored and purple-colored contours denote the storm-height temperatures beyond and below 0°C, respectively. Boxes shown in the figure indicate the sites listed in Table 1.